scientific reports

Check for updates

OPEN

Regulation viral RNA transcription and replication by higher-order RNA structures within the nsp1 coding region of MERS coronavirus

Yutaka Terada[1,2], Sodbayasgalan Amarbayasgalan[3], Yoshiharu Matsuura[4,5,6] & Wataru Kamitani[1,3]✉

Coronavirus (CoV) possesses numerous functional cis-acting elements in its positive-strand genomic RNA. Although most of these RNA structures participate in viral replication, the functions of RNA structures in the genomic RNA of CoV in viral replication remain unclear. In this study, we investigated the functions of the higher-order RNA stem-loop (SL) structures SL5B, SL5C, and SL5D in the ORF1a coding region of Middle East respiratory syndrome coronavirus (MERS-CoV) in viral replication. Our approach, using reverse genetics of a bacterial artificial chromosome system, revealed that SL5B and SL5C play essential roles in the discontinuous transcription of MERS-CoV. In silico analyses predicted that SL5C interacts with a bulged stem-loop (BSL) in the 3′ untranslated region, suggesting that the RNA structure of SL5C is important for viral RNA transcription. Conversely, SL5D did not affect transcription, but mediated the synthesis of positive-strand genomic RNA. Additionally, the RNA secondary structure of SL5 in the revertant virus of the SL5D mutant was similar to that of the wild-type, indicating that the RNA structure of SL5D can finely tune RNA replication in MERS-CoV. Our data indicate novel regulatory mechanisms of viral RNA transcription and replication by higher-order RNA structures in the MERS-CoV genomic RNA.

Coronaviruses (CoVs) (order Nidovirales, family Coronaviridae, subfamily Coronavirinae) are enveloped and contain large single-stranded, positive-sense RNA. Most CoVs cause enteric and/or respiratory diseases in both mammals and birds[1]. In humans, most CoVs cause mild illnesses, including the common cold[2–5]. Three lethal human CoVs have emerged as zoonotic pathogens within this century. One is the severe acute respiratory syndrome CoV (SARS-CoV), which emerged in 2002 in China[6,7], and second is the Middle East respiratory syndrome CoV (MERS-CoV), which emerged in Saudi Arabia in 2012[8]. MERS-CoV remains endemic, with more than 2000 cases and 858 deaths reported. Third, most recently, coronavirus disease 2019 (COVID-19), caused by SARS-CoV-2, became a global pandemic[9–11].

Numerous RNA viruses utilize functional RNAs in their genomes as cis-acting elements for efficient viral replication[12–15]. One of the most well-known functional RNA structures is the internal ribosome entry site (IRES)[16,17], which induces efficient translation of viral proteins by directly recruiting the host translational system. As CoVs have the largest RNA genome among all RNA viruses, they possess several types of RNA structures[18,19]. The stem-loop (SL) structure within the non-structural protein 15 (nsp15)-coding region of the mouse hepatitis virus (MHV) acts as a packaging signal[20]. Similar to other viruses, higher-order RNA structures within the 5′ or 3′ untranslated region (UTR) of the CoV genome have been proposed to be cis-acting elements[21–26]. We discovered that nsp1 from SARS-CoV and MERS-CoV are RNA-binding proteins that bind and utilize the SL1 region within the 5′ UTR of viral RNA as a gene marker for viral RNA. This recognition plays an important role in evading translational shutoff and RNA degradation induced by nsp1[27,28]. RNA structures in CoV genomic RNA have been proposed to act as cis-acting elements for replication based on experiments using defective

[1]Laboratory of Clinical Research on Infectious Diseases, Research Institute for Microbial Diseases, Osaka University, Suita, Japan. [2]Center for Vaccine Research and Department of Immunology, University of Pittsburgh, Pittsburgh, PA, USA. [3]Department of Infectious Diseases and Host Defense, Graduate School of Medicine, Gunma University, Maebashi, Japan. [4]Center for Infectious Disease Education and Research (CiDER), Suita, Japan. [5]Research Institute for Microbial Diseases (RIMD), Suita, Japan. [6]Center for Advanced Modalities and DDS (CAMaD), Osaka University, Suita, Japan. ✉email: wakamita@gunma-u.ac.jp

interfering (DI)-RNA[22,24,25,29]. However, the detailed mechanisms through which cis-acting RNA in the CoV genome regulate viral replication remain unclear.

Recently, we used a reverse genetics approach in a bacterial artificial chromosome (BAC) system and discovered that RNA structures of the SL5 region in MERS-CoV RNA participate in viral replication[28]. The SL5 RNA region, which consists of SL5B, SL5C, and SL5D, encodes the 5′ UTR and the nsp1 coding region. However, the infectious virus could not be recovered from the cDNA clone because of an amino acid substitution at position 13 of nsp1 in the SL5 region, which disrupted the RNA structure and impaired viral replication. In contrast, the cDNA clone that retained the RNA structure of SL5 produced an infectious virus. Our previous results suggest that higher-order RNA structures in SL5 of the MERS-CoV genome play critical roles in viral replication. Although the importance of RNA structures for viral replication has been discussed, the functions of specific RNA structures during the CoV life cycle remain unclear.

In this study, we examined the biological effects of RNA structures in SL5 of the MERS-CoV genome on viral RNA transcription and replication using a reverse genetics approach in a BAC system. Our mutant viruses showed that the RNA structures of both SL5B and SL5C were important for the production of subgenomic mRNAs. In contrast, the RNA structure of SL5D proved to be critical for the replication of positive-stranded genomic RNA. Our results suggest that the higher-order RNA structures of SL5 in the MERS-CoV RNA genome play critical roles in regulating RNA transcription and replication during the viral life cycle.

Results

Effects of higher-order RNA structures, SL5B, SL5C, and SL5D in viral propagation

In a previous report, the RNA sequence consisting of SL5B, SL5C, and SL5D within the nsp1-coding region was shown to likely function as a cis-acting element in viral propagation[28]. To examine the roles of SL5B, SL5C, and SL5D in viral propagation, we constructed cDNA clones carrying mutations in these regions (Fig. 1A,B). The SL5B-Loop and SL5C-Loop mutants (pBAC-MERS-SL5B-Loop and pBAC-MERS-SL5C-Loop, respectively) were designed to retain their RNA structures within the loop regions. SL5B-R, SL5C-R, and SL5D-R, which contain mutations on the right side of each stem region, were designed to disrupt the RNA structures (pBAC-MERS-SL5B-R, pBAC-MERS-SL5C-R, and pBAC-MERS-SL5D-R, respectively). To retain the secondary RNA structures

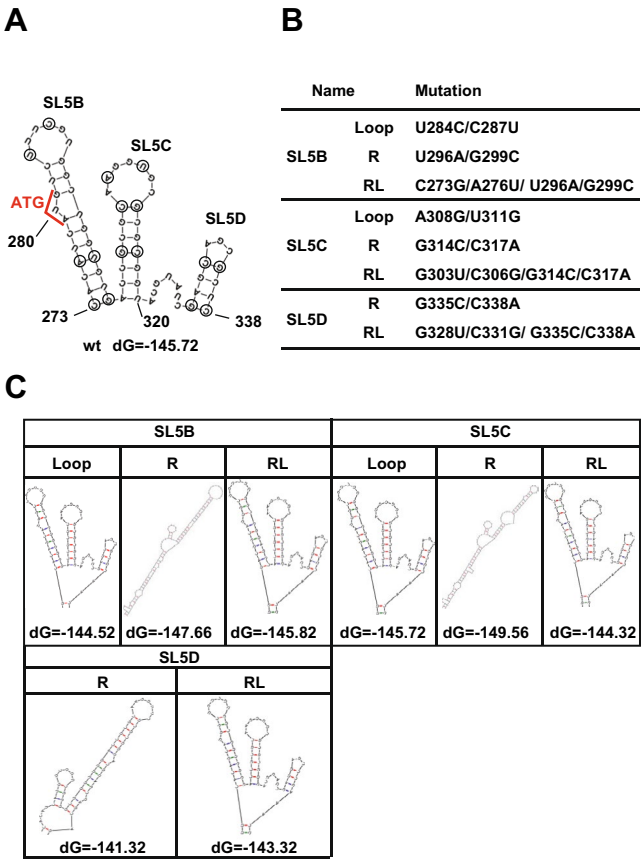

Fig. 1. Construction of SL5 structure disrupting mutants. (**A**) RNA structures predicted by Mfold. Numbers indicate the nucleotide positions in the MERS-CoV EMC strain (DDBJ accession No. NC_019843). Circles indicate the mutation sites for each of the SL5 mutants shown in (**B**). ATG: Start codon of ORF1a. (**B**) Nucleotide mutations of SL5B, SL5C, and SL5D mutants used in this study. (**C**) Predicted secondary RNA structures of each mutant.

in each SL, mutations were introduced to the left side of each stem region, yielding SL5B-RL, SL5C-RL, and SL5D-RL (pBAC-MERS-SL5B-RL, pBAC-MERS-SL5C-RL, and pBAC-MERS-SL5D-RL, respectively). Nucleotide substitutions in SL5C-RL and SL5D-RL caused non-synonymous mutations in the nsp1 protein. The secondary RNA structures of the mutants used in this study using Mfold analysis[30] are shown in Fig. 1C. As expected, SL5B-Loop, SL5B-RL, SL5C-Loop, SL5C-RL, and SL5D-RL retained the same RNA structure as their wild-type (WT) counterparts. In contrast, SL5B-R, SL5C-R, and SL5D-R were predicted to disrupt the RNA structures of SL5.

To investigate the functional significance of SL5 structures in viral propagation, we transfected full-length cDNA clones of either WT or mutant viruses into Huh7 cells, and viral titers in the culture supernatants were determined using a 50% tissue culture infectious dose ($TCID_{50}$) assay with Vero cells (Fig. 2A). Viral infectivity in cells transfected with pBAC-MERS-WT reached 3.16E+05 $TCID_{50}$/mL 72 h post-transfection. Although the viral infectivity levels in cells transfected with pBAC-MERS-SL5B-Loop and pBAC-MERS-SL5B-RL were low at 48 h post-transfection, both values increased to approximately 1.0E+04 $TCID_{50}$/mL at 72 h post-transfection (Fig. 2A). In particular, there was a statistically significant (two-way ANOVA) difference in the infectious virus titer in the 5B-R, 5C-R, and 5D-R samples at 72 h compared to the WT. The predicted RNA secondary structures of SL5B-Loop and SL5B-RL indicated that both mutants retained the RNA secondary structure from nts 1–460, which contains the nsp1-coding region (Fig. 1C). In contrast, the SL5B-R mutation disrupted the RNA secondary structure (Fig. 1C). In combination with our finding that no viral progeny was recovered from the pBAC-MERS-SL5B-R transfected cells (Fig. 2A), data suggest that the RNA structure of SL5B is important for efficient viral replication.

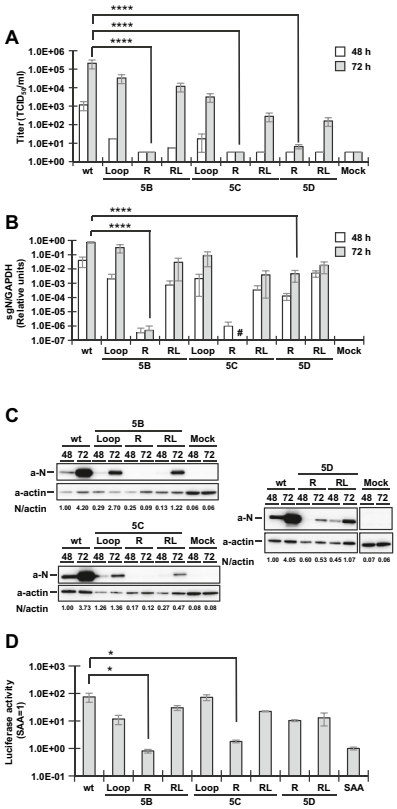

Fig. 2. Effects of SL5B, SL5C, and SL5D RNA structures on viral propagation. (**A**) Viral growth of SL5 mutants. Huh7 cells were transfected with the MERS-CoV cDNA clones and cultured. Experiments were carried out in triplicate and representative results were shown. Culture supernatants were collected to harvest the virus, and viral titers were determined by $TCID_{50}$ assay using Vero cells. Mock indicates the transfected Huh7 cells with backbone BAC plasmid without any viral sequence. **** $P < 0.0001$. (**B**) Real-time RT-PCR results evaluating viral RNA transcription. Huh7 cells transfected with each cDNA clone were cultured for the indicated times. Total RNA was extracted from each infected cell, and real-time RT-PCR targeting sg N mRNA was performed. The sg N mRNA levels were normalized to the GAPDH mRNA levels. **** $P < 0.0001$. # represents the limit of detection. (**C**) Immunoblot analysis for the detection of MERS-CoV N protein. Cell lysates of Huh7 cells transfected with each cDNA clone were subjected to western blot analysis using anti-MERS-CoV N antibody (a-N) and anti-actin antibody (a-Actin). (**D**) Luciferase activities of replicons carrying each of the SL5 mutants. 293T cells were transfected with each cDNA replicon and cultured for 48 h. Nluc activities in cultured cells were measured using confocal microscopy. Firefly luciferase activities from pGL3-control plasmid were also measured as an internal control. Polymerase dead mutant (SAA) was used as a negative control.* $P < 0.05$.

As shown in Fig. 2A, SL5C mutants presented features similar to those of SL5B. Both SL5C-Loop and SL5C-RL produced viral progeny in the culture supernatants, whereas SL5C-R, which had a disrupted secondary structure, produced no viral progeny (Figs. 1C and 2A). As expected, SL5D-RL, which retained its RNA secondary structure, produced viral progeny (Fig. 2A). Unlike SL5B-R and SL5C-R, SL5D-R released viral progeny into the culture supernatant; however, the viral titer was lower than that of the WT construct (Fig. 2A). These results suggest that the RNA structures of SL5B, SL5C, and SL5D are important for efficient viral propagation, and that the SL5D structure regulates viral propagation through an unknown mechanism that is different from that of SL5B and SL5C.

Effect of SL5 RNA secondary structure on viral RNA transcription and viral protein expression

To examine the functional significance of SL5 RNA secondary structures in viral RNA transcription, we extracted total RNA from Huh7 cells transfected with cDNA clones and performed real-time RT-PCR to measure the expression levels of subgenomic (sg) mRNA for nucleocapsid (N) protein (sg N mRNA) (Fig. 2B). As expected, the four mutants that retained their RNA secondary structures, SL5B-Loop, SL5B-RL, SL5C-Loop, and SL5C-RL–efficiently produced sg N mRNA (Fig. 2B). In contrast, the mutants with disrupted RNA secondary structures, SL5B-R and SL5C-R, did not produce sg N mRNA (Fig. 2B). A statistically significant difference (two-way ANOVA) was observed between the amount of 5B-R and 5D-R viral RNA at 72 h compared to the WT. Notably, the amount of 5C-R viral RNA was below the detection limit. Although the infectious viral titers in pBAC-MERS-SL5D-R-transfected cells were substantially lower than those in pBAC-MERS-SL5D-RL-transfected cells (Fig. 2A), the expression levels of sg N mRNA in pBAC-MERS-SL5D-R-transfected cells were similar to those in the SL5D-RL mutant (Fig. 2B). These results indicate that the disruption of SL5B and SL5C, but not SL5D, reduces sg N mRNA transcription.

Next, we measured the expression levels of the viral N protein in Huh7 cells transfected with cDNA clones using immunoblotting (Fig. 2C). The amount of N protein increased in pBAC-MERS-WT-transfected cells in a time-dependent manner. N protein expression was detected in cells transfected with SL5B-Loop, SL5B-RL, SL5C-Loop, and SL5C-RL at 72 h post-transfection. However, the levels of the N protein were lower than those in cells expressing the WT virus (Fig. 2C, left panels). In contrast, no expression of the N protein was observed in cells expressing the RNA-disrupting mutants SL5B-R and SL5C-R (Fig. 2C, left panels), which was due to a significant reduction in sg N mRNA production (Fig. 2B). Unlike SL5B-R and SL5C-R mutants, the SL5D-R mutant produced the N protein (Fig. 2C, right panel); however, the amount of N protein produced was lower than that in cells expressing SL5D-RL (Fig. 2C, right panels). These results suggest that the RNA structures in SL5 regulate the transcription of sg N mRNA.

To confirm the functional significance of the SL5 RNA structure in viral RNA transcription, we used a MERS-CoV RNA replicon system in which MERS-CoV RNA efficiently replicates but does not produce any infectious particles. The MERS-CoV replicon system was engineered to contain the nano luciferase (Nluc) gene and the TRS-M 100 nt upstream of the Nluc gene to increase Nluc expression (designated pBAC-MERS-Rep). As a negative control, we used a replicon cDNA clone containing dead RNA-dependent RNA polymerase (RdRP; nsp12). To generate a series of MERS-CoV replicon cDNA clones with SL5 mutants, pBAC-MERS-Rep was used as the template. Consistent with the expression levels of sg N mRNA (Fig. 2B), luciferase activity in 293T cell lysates at 48 h post-transfection with replicon cDNA, excluding SL5B-R and SL5C-R, was significantly increased (Fig. 2D). There was also a significant difference in the amount of replication of the replicon DNA of 5B-R and 5C-R as compared to that of the WT. These results suggest that the RNA structures of SL5B and SL5C, but not that of SL5D, play critical roles in viral RNA transcription. In contrast, the RNA structure of SL5D may function only after viral RNA transcription.

Effects of SL5B and SL5C RNA structures on viral RNA transcription

Using a reverse genetics system for MERS-CoV, we discovered that mutations in SL5B-R and SL5C-R arrested the viral RNA transcription (Fig. 2B). This may be due to the low stability of the genomic RNA conferred by the introduction of nucleotide substitutions. To test this possibility, we evaluated the levels of genomic RNA at earlier time points after the transfection of WT, SL5B-R, SL5B-RL, SL5C-R, and SL5C-RL cDNA into Huh7 cells. Based on real-time RT-PCR analyses, the expression levels of genomic RNA at 0, 4, 8, and 12 h post-transfection were similar in all conditions (Fig. 3A); thus, suggesting that nucleotide substitutions in SL5B and SL5C did not affect viral genomic RNA stability.

In the CoV lifecycle, after uncapsidation, genomic RNA functions as an mRNA to produce nsps that are critical for subsequent viral RNA transcription and replication[31]. Next, we tested the effects of nucleotide substitutions in SL5B or SL5C on genomic RNA translation using a firefly luciferase reporter plasmid carrying nts 265–348 of MERS-CoV, including SL5B, SL5C, and SL5D, upstream of the firefly luciferase gene (Fig. 3B). A reporter plasmid without the viral sequence was used as a control (fluc). Luciferase activity in 293T cells at 24 h post-transfection indicated that the levels in all SL5 mutants were comparable to those associated with the WT sequence (SL5) (Fig. 3C). These results indicated that nucleotide substitutions in SL5B and SL5C did not affect genomic RNA translation.

As shown in Fig. 3A,C, the impairment of viral RNA replication by SL5B-R and SL5C-R cDNA was not due to decreased RNA stability or loss of genomic RNA translation. Next, we investigated whether the secondary RNA structures of SL5B and SL5C affected viral nsp(s) expression using a luciferase-based biosensor system to detect nsp5 protease activity, as shown in Fig. 3D[32]. The specific amino acid sequence (VRLQS) recognized and cleaved by MERS-CoV nsp5 was inserted into a firefly luciferase reporter plasmid to produce pGlo-30F-VRLQS[32]. Luciferase activities of Huh7 cells co-transfected with pGlo-30F-VRLQS and MERS-CoV cDNA clones are shown in Fig. 3E. Similar to the WT, all SL5B and SL5C mutants showed increased luciferase activity, suggesting

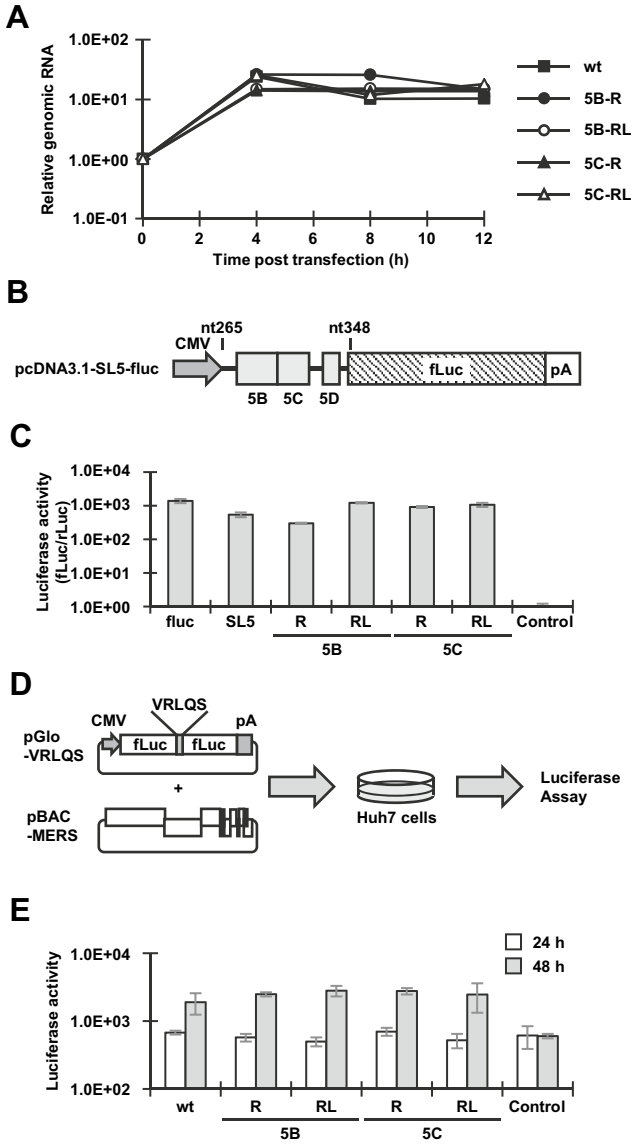

Fig. 3. Functional step of SL5B and SL5C in MERS-CoV lifecycle. (**A**) Genomic RNA stabilities of viruses containing mutant SL5B or SL5C regions with disrupted secondary structures. Huh7 cells were transfected with each cDNA clone and cultured for 0, 4, 8, and 12 h. Total RNA were extracted from the cells and subjected to real-time RT-PCR targeting ORF1a region to measure the levels of genomic RNA. The levels of genomic RNAs were normalized to the GAPDH mRNA levels. (**B**) Schematic of pcDNA3.1-SL5-fluc plasmid. MERS-CoV sequence from nts 265–343 was inserted between the CMV promoter and the firefly luciferase gene (fluc). Gray squares indicate the nucleotide regions of SL5B, SL5C, and SL5D. (**C**) Effects of SL5B and SL5C structures on protein translation. 293T cells were transfected with pcDNA3.1-SL5-fluc or SL5B/SL5C mutants. pcDNA3.1-fluc without the viral sequence was used as a positive control. Renilla luciferase reporter plasmid, pRL-SV40, was used as the internal control. After 24 h of incubation, the transfected cells were collected, and luciferase activities were measured. Firefly luciferase activities were normalized to the Renilla luciferase activities. (**D**) Schematic diagram of the reporter assay for detecting the MERS-CoV protease, nsp5. cDNA clones of WT, SL5B mutant, or SL5C mutant were co-transfected into Huh7 cells with the pGlo-VRLQS biosensor plasmid. Translated proteins from pGlo-VRLQS do not show luciferase activity. Cleavage caused by MERS-CoV nsp5 increases luciferase activity. Transfected Huh7 cells were cultured for 24 and 48 h, and luciferase activities in cells were measured using confocal microscopy. (**E**) Expression of nsp5 in SL5B and SL5C mutants. The results of the MERS-CoV nsp5 biosensor assay described in (**D**). The Nsp5 deletion mutant, pBAC-MERS-nsp5-rpsL, was used as a negative control (Control).

that nucleotide substitutions in SL5B and SL5C did not impair genomic RNA translation. Thus, the structures of SL5B and SL5C are key factors in viral RNA transcription after the first round of translation and they play a role in nsps production.

Identification of the RNA-RNA interaction region between SL5 and 3′ UTR

In several positive-stranded RNA viruses, RNA-RNA interactions in genomic RNA are important for regulating viral RNA transcription or translation[33]. As shown in (Figs. 1, 2, 3), the RNA structures of SL5B and SL5C regulate viral RNA transcription. To identify the RNA-RNA interaction sites of SL5 in the genomic RNA of MERS-CoV, we used the LRIscan software[33]; 30,258 RNA-RNA interactions were predicted to occur within the MERS-CoV genome (Fig. 4A). Although the p-value above a commonly used threshold (0.277) (Fig. 4B), the stem region of SL5C (nts 301–305) was predicted to interact with the bulged stem-loop (BSL, nts 29,829–29,833) of the 3′ UTR (Fig. 4B). These results suggest that SL5C may play an important role in regulating viral RNA transcription through the circularization of genomic RNA via its interaction with the BSL in the 3′ UTR.

SL5D regulates positive-strand genomic RNA replication

Although the infectious viral titer was low in pBAC-MERS-SL5D-R-transfected Huh7 cells (Fig. 2A), the expression levels of sg N mRNA and protein were comparable to those in pBAC-MERS-SL5D-RL-transfected cells (Fig. 2B,C). Furthermore, RNA transcription and replication occurred efficiently in the SL5D-R replicon DNA-transfected cells (Fig. 2D). These results led us to hypothesize that viral assembly was impaired in the pBAC-MERS-SL5D-R-transfected cells. We further believe that the identification of infected cells in the SL5D-R sample was difficult because of the low infectious viral titer in the pBAC-MERS-SL5D-R-transfected cells (Fig. 2A).

To overcome this difficulty, we used confocal microscopy to identify infected cells using reporter viruses carrying the fluorescent protein ZsGreen (data not shown). In addition, we utilized transmembrane serine protease 2 (TMPRSS2)-expressing Vero-TMPRSS2 cells[34] to obtain a reasonable amount of rMERS-ZsGreen virus containing the SL5D-R mutation for transmission electron microscopy (TEM) analysis. The infectious viral titer of the WT and mutant viruses was higher in Vero-TMPRSS2 cells than that in Vero cells (data not shown). Vero cells inoculated with WT or SL5D-R reporter viruses (MOI = 0.1) were cultured for 24 h and fixed to identify infected cells by confocal microscopy. The infected cells were subsequently analyzed using TEM. As shown in Fig. 5B, the SL5D-R virus particles were approximately 100 nm in size, similar to those observed in infected WT cells. These results suggest that viral particles were produced in SL5D-R-infected cells.

Next, we evaluated the effects of the SL5D secondary structure on viral release from infected cells by inoculating Vero cells with either rMERS-ZsGreen or rMERS-ZsGreen-SL5D-R and measuring viral titers in the culture supernatants. The viral release was calculated by dividing the infectious viral titer in the culture supernatants by that in the cells (Fig. 5C). Statistically, there was a significant difference in the amount of virus released into the supernatant of the cells infected with the WT and SL5D-R virus. Although the viral release from cells infected with the WT virus increased in a time-dependent manner, no increase was observed for the SL5D-R-infected cells (Fig. 5C). These results suggest that the loss of the secondary structure in SL5D attenuates viral release.

Although viral particles were observed in the SL5D-R infected cells (Fig. 5B), the amount of virus released from the infected cells was low (Fig. 5C). Next, we examined the amount of positive-strand viral genomic RNA in SL5D-R-infected cells using real-time RT-PCR. Because positive-stranded genomic RNA is incorporated into infectious viral particles, we hypothesized that the loss of viral release was due to the decreased production of genomic RNA in SL5D-R-infected cells. To test this hypothesis, Huh7 cells transfected with pBAC-MERS-wt or pBAC-MERS-SL5D-R were cultured for 72 h, and total RNA was extracted and subjected to real-time RT-PCR

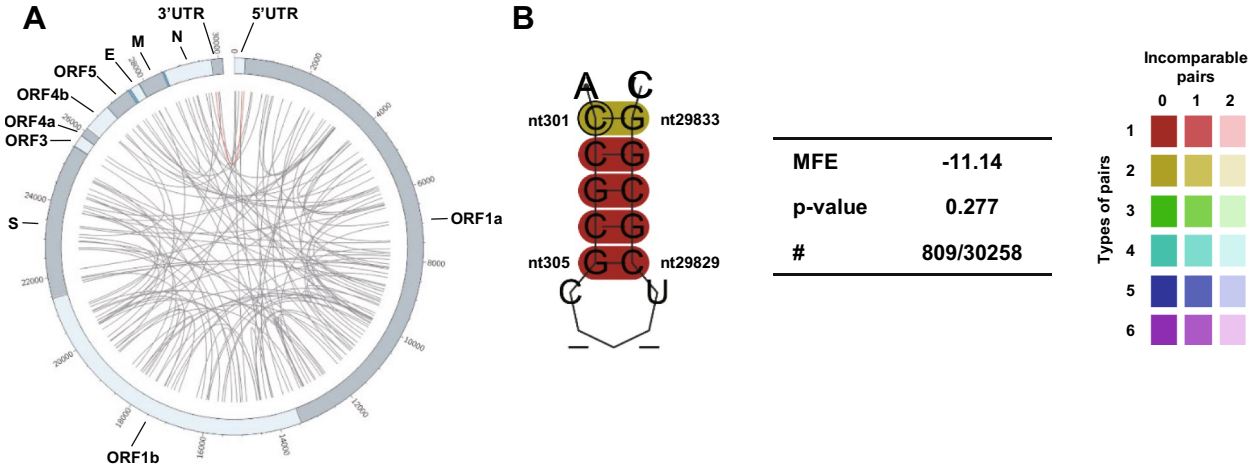

Fig. 4. Prediction of long RNA-RNA interaction with SL5. (**A**) Plot of all predicted LRI values with $P < 0.005$ observed in four MERS-CoV genomes. The outer circle represents the genome information of MERS-CoV. The inner circle shows all predicted interactions between all genome positions. The plot was created with Circos[50]. (**B**) Predicted RNA-RNA interaction between SL5C and the BSL within the 3′UTR based on the LRIscan analysis. The nucleotide positions in MERS-CoV EMC are indicated (DDBJ accession No. NC_019843).

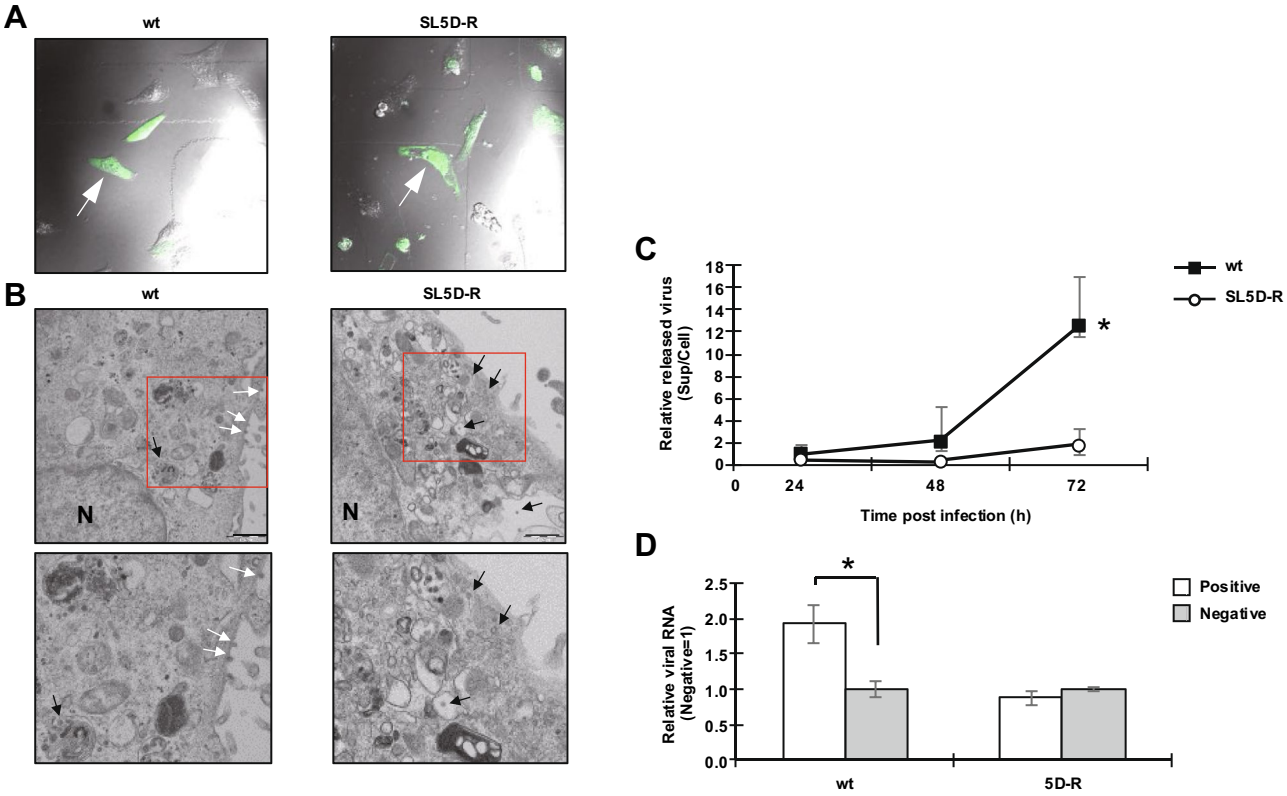

Fig. 5. Functional step of SL5D in MERS-CoV lifecycle. (**A**, **B**) Correlative light and electron microscopy (CLEM) analysis of rMERS-ZsGreen or rMERS-ZsGreen-SL5D-R mutants. Vero cells were inoculated with rMERS-ZsGreen or rMERS-ZsGreen-SL5D-R (MOI = 0.1) and cultured for 24 h. (**A**) Infected cells were identified by green fluorescence and (B) subjected to transmission electron microscopy (TEM) analysis. Black arrows indicate the viral particles inside the infected cells. White arrows indicate the viral particles on the cell surface. Scale bar = 1 µm. *N* nucleolus. Bottom: Zoomed image of red square areas from top TEM image. (**C**) Viral release of rMERS-ZsGreen or rMERS-ZsGreen-SL5D-R mutants from Vero cells. Vero cells were inoculated with rMERS-ZsGreen or rMERS-ZsGreen-SL5D-R (MOI = 0.01) and cultured. At the indicated time, culture supernatants were collected. Cells were collected in fresh medium, stored frozen, and then thawed before use. Viral titers of both supernatants (Sup) and cell (Cell) samples were measured to determine the levels of released virus relative to that inside the cell. * $P < 0.05$ (**D**) Examination of the levels of strand-specific genomic RNA in wildtype or the SL5D-R mutant virus. Huh7 cells were transfected with pBAC-MERS or pBAC-MERS-SL5D-R and cultured for 72 h, and total RNAs were extracted. RNA samples were reverse-transcribed using positive- or negative-strand specific primers and then treated with RNaseH. The strand-specific cDNAs were subjected to real-time PCR targeting the ORF1a region. * $P < 0.05$.

to detect either positive- or negative-strand genomic RNA. The amount of positive-strand genomic RNA was divided by that of the negative-strand genomic RNA. As shown in Fig. 5D, the amount of positive-stranded genomic RNA relative to negative-stranded genomic RNA in cells transfected with pBAC-MERS-WT was > 1.0, which was a statistically significant increase. In contrast, the value in pBAC-MERS-SL5D-R-transfected cells was 1.0, indicating that the synthesis of positive-strand genomic RNA was impaired in SL5D-R-infected cells. These results suggest that the structure of SL5D plays an important role in the synthesis of positive-stranded genomic RNA.

Emergence of revertant virus from SL5D-R

Although the infectious viral titer in the culture supernatants released from pBAC-MERS-SL5D-R-transfected Huh7 cells was low, we successfully recovered the mutant virus from these cells (Fig. 2A). To understand the biological significance of the SL5D structure in viral RNA replication, we sought to obtain a revertant virus by serially passaging Vero cells. Although the cytopathic effect (CPE) was still weak in infected Vero cells at passages 1 and 2, it became much stronger in cells after passage 10. The nucleotide sequences of the SL5D mutation sites in the P1, P2, P5, and P10 virus samples were examined. Although the introduced mutation (G335C/C338A) in SL5D-R was retained in the P1 and P2 viruses, a revertant mutation (C338) at position 338 was identified in the P5 virus (Fig. 6A,B). Additionally, the revertant mutation (C338) was predominant after passage 10 (Fig. 6B). The C population reached 50% (5/10), as shown in Fig. 6B. The emergence of the revertant virus indicates that the SL5D structure has beneficial effects on MERS-CoV propagation.

Next, we investigated the growth of the passaged SL5D-R virus in Vero cells. Vero cells inoculated with P2, P5, or P10 viruses (MOI = 0.01) were cultured for 24, 48, and 72 h, and infectious viral titers in the supernatants

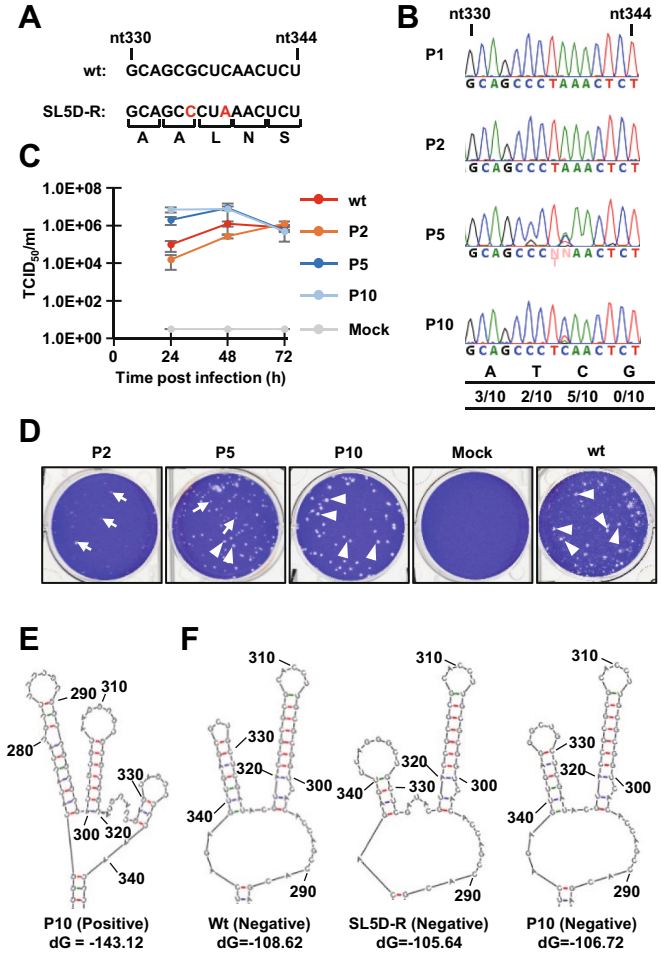

Fig. 6. Emergence of revertant SL5D-R mutant virus in Vero cells. (**A**) Nucleotide sequences from 330–344 of WT and SL5D-R mutant viruses. Mutated nucleotides are shown in red. (**B**) Nucleotide sequences of rMERS-SL5D-R viruses passaged in Vero cells. Vero cells were inoculated with rMERS-SL5D-R virus and passaged. After ten passages in Vero cells, viral RNAs were extracted from the P1, P2, P5, and P10 virus stocks, and RT-PCR was performed to amplify the SL5D region and read the nucleotide sequences. The amplified PCR products were cloned into a Blunt vector and transformed to *E. coli*. The cloned vector DNA from ten clones was extracted and the nucleotide sequences were identified. (**C**) Growth kinetics of passaged rMERS-SL5D-R viruses in Vero cells. Vero cells were inoculated with rMERS or passaged rMERS-SL5D-R viruses (MOI = 0.01) and cultured. Viral titers of culture supernatants were determined using the $TCID_{50}$ assay. (**D**) Plaque morphology of the passaged rMERS-SL5D-R viruses. Seeded Vero cells were inoculated with 25 $TCID_{50}$ of each virus. Infected Vero cells were fixed with phosphate-buffered formaldehyde at 3 d post infection and stained using crystal violet. White arrow indicates small plaques. White arrowheads indicate large plaques. Scale bar = 1 cm. (**E**) RNA structures of positive-strand RNA of P10 virus predicted following Mfold analysis. (**F**) RNA structures of negative-strand RNA predicted following Mfold analysis. Predicted structures were constructed using the reverse-complement sequences of nts 1–460 from the WT, SL5D-R mutant, and SL5D-R P10 viruses. Numbers indicate the corresponding nucleotide position of positive-strand genomic RNA.

were measured. The results show that the highly passaged viruses (P5 and P10) exhibited increased growth kinetics compared to the low-passage virus P2 (Fig. 6C). The P2 virus produced the smallest plaques, the P5 virus produced both small and large plaques, and the P10 virus produced large plaques (Fig. 6D). Thus, plaque size correlated with the ratio of revertant to non-revertant viruses (Fig. 6B). These results suggest that the RNA structure of SL5D is important for efficient viral replication as it regulates the synthesis of positive-strand genomic RNA.

To clarify the molecular mechanisms underlying efficient viral replication in cells infected with the revertant virus (P10 virus), we predicted the RNA secondary structure of SL5D in the P10 virus using Mfold. As expected, the predicted RNA structures of the positive and negative strands of the P10 virus were analogous to those of the WT virus (Fig. 6E,F, right panel). Furthermore, the predicted RNA secondary structure of the negative strand of SL5D-R was different from that of the WT and P10 viruses (Fig. 6F). As shown in Fig. 6F, one stem-loop structure within the negative-strand RNA corresponding to the SL5D region (nts 328–338) was predicted for all three viruses (WT, SL5D-R, and P10). A short stem-loop with a stem structure consisting of seven base pairs was predicted in the negative strand of the WT virus. In contrast, the stem structure in the short stem-loop of the negative-strand of SL5D-R consisted of four base pairs (Fig. 6F, middle panel), whereas this structure consisted

of six base pairs in the P10 virus (Fig. 6F, right panel). This suggests that the stem-loop structure of SL5D in the negative-strand is important for regulating positive-strand genomic RNA synthesis.

Discussion

Several studies had reported the importance of RNA structures at the 5′ UTR, its adjacent ORF1a coding region, and the 3′ UTR of CoV genomes for viral and/or DI-RNA replication[21,24,25,35,36]. However, the detailed functions of these RNA structures in the viral life cycle have not yet been fully elucidated. In this study, we revealed the significant roles of the higher-order RNA structures SL5B, SL5C, and SL5D in the MERS-CoV lifecycle using a BAC-based reverse genetics system. Our results show that SL5B and SL5C play essential roles in regulating viral RNA transcription to synthesize sg mRNAs (Fig. 3). In contrast, SL5D is important for regulating the synthesis of the positive-strand genomic RNA (Fig. 5).

Higher-order RNA structures in viral genomic RNA are important for increasing its stability and evading host RNA degradation machinery[37,38]. We hypothesized that disrupting the RNA structure of the SL5 impairs viral replication by decreasing the stability of viral genomic RNA. However, the levels of genomic RNA in cells transfected with mutant viruses lacking the secondary structure (SL5B and SL5C) were similar to those in the WT (Fig. 3A); thus, suggesting that the higher-order structures in these regions do not directly affect genomic RNA stability. Furthermore, our luciferase reporter assay indicated that the disruption of RNA structures in the SL5B and SL5C mutants did not impair the translational ability of their own mRNAs (Fig. 3C). The protease activity of nsp5 in cells transfected with SL5B or SL5C mutant cDNA was similar to that in cells transfected with WT cDNA (Fig. 3E). Thus, the RNA structures of SL5B and SL5C are responsible for regulating viral RNA transcription during the MERS-CoV life cycle.

CoV has been shown to synthesize sg mRNAs via discontinuous transcription, which is a unique mechanism[39]. Given the lack of sg N mRNA, the RNA structures of SL5B and SL5C are essential for sg N mRNA synthesis. In this discontinuous transcription model, the transcription regulatory sequence (TRS) located at the leader sequence (TRS-L) and preceding each viral gene (TRS-B) plays a critical role in mediating long RNA-RNA interactions (leader-body joining) and switching the template[40–42]. Circularization of the CoV genome through the interaction between the 5′ and 3′UTRs is important for forming the leader-body joining and subsequent viral RNA elongation[42]. We predicted a specific interaction between SL5C and BSL at the 3′UTR (Fig. 4). Although further studies are required to investigate the interaction between SL5C and BSL, our results suggest that the RNA structure of SL5C is critical for the circularization of viral genomic RNA. Although a binding interaction was not predicted for SL5B, the SL5B disrupting mutant showed a phenotype similar to that of the SL5C mutant. These results indicate that the RNA structure of SL5B neighboring SL5C may affect the interaction between SL5C and BSL.

CoVs use both host proteins and viral proteins to replicate and transcribe viral RNA. Poly A binding protein is involved in the RNA circularization of CoV[43], and the viral N proteins of the MHV and the transmissible gastroenteritis virus participate in viral RNA transcription through RNA-RNA interactions between TRS-L and TRS-Bs[44–46]. The MHV N protein also interacts with RNA sequences to modulate the packaging of MHV genomic RNA[47]. Although further studies are needed to identify the host factor(s) or viral proteins that interact with the SL5 region of MERS-CoV, our results suggest that these higher-order RNA structures interact with the host and/or viral proteins to play important roles in viral RNA transcription and replication. Our data indicates that the RNA structures of SL5 have drastic effects on MERS-CoV replication; hence, host proteins that interact with SL5 are attractive candidates for developing therapeutic agents against MERS-CoV infection.

Interestingly, SL5D mutants showed a different phenotype than that of SL5B and SL5C mutants (Fig. 2), even though SL5D is adjacent to both SL5B and SL5C in the MERS-CoV genomic RNA. Although the SL5D-R mutant synthesized sg mRNA, it did not efficiently produce viral progeny (Fig. 2A,B). These results indicate that SL5D functions at a different step in the viral lifecycle than SL5B and SL5C. Our results suggested that SL5D is important for the synthesis of positive-strand genomic RNAs (Fig. 5C). In addition, we recovered a revertant SL5D-R virus. We introduced two nucleotide substitutions (G335C and C338A) into the SL5D region to construct the SL5D-R mutant (Fig. 1B); however, the P10 virus acquired one revertant substitution at position 338 (Fig. 6B). As expected, the predicted RNA secondary structure of the positive-strand RNA in SL5 of the P10 virus was similar to that of the WT (Fig. 6E). Furthermore, the negative-strand RNA of the WT and passaged P10 viruses was predicted to contain longer stem-loop structures within SL5D than those associated with the SL5D-R mutant (Fig. 6F). Thus, the stem-loop structure of the negative-strand RNA in the region corresponding to SL5D is important for regulating the synthesis of genomic (positive-strand) RNA from negative-strand RNA.

In conclusion, we identified that higher-order RNA structures within the nsp1 coding region play critical roles in the MERS-CoV lifecycle through several steps. Our approach using a BAC-based reverse genetics system revealed that higher-order RNA structures within viral RNA regulate viral RNA transcription and replication. Furthermore, these RNA structures are conserved among betacoronaviruses despite their low nucleotide homology[19,21,48], thereby suggesting that these RNA structures are potential targets for developing novel antivirals against betacoronaviruses. Further studies are required to reveal the mechanisms through which the highly structured SL5 RNA regulates CoV RNA transcription and replication through RNA-RNA and/or RNA–protein interactions.

Methods

Cells and viruses

Huh7 (human hepatocellular carcinoma, JCRB0403 from JCRB cell bank) and 293T (human embryonic kidney, CRL-3216 from ATCC) cells were maintained in Dulbecco's modified minimum essential medium (DMEM) (Nacalai Tesque, Kyoto, Japan) containing 10% heat-inactivated fetal bovine serum (FBS), 100 U/mL penicillin,

and 100 µg/mL streptomycin (Nacalai Tesque). Vero cells (African green monkey kidney) and Vero-TMPRSS2[34] were maintained in DMEM containing 5% FBS, 100 U/mL penicillin, and 100 µg/mL streptomycin (Nacalai Tesque). Vero-TMPRSS2 cells were a kind gift from Dr. Shutoku Matsuyama (National Institute of Infectious Diseases, Tokyo, Japan). Cells were cultured in a humidified, 5% CO_2 atmosphere at 37 °C.

BAC construction

We previously established a reverse genetics system for MERS-CoV using the BAC system: pBAC-MERS-WT[28]. To construct cDNA clones of several SL5 mutants from pBAC-MERS-WT, we used the Red/ET Recombination System Counter-Selection BAC Modification Kit (Gene Bridges, Heidelberg, Germany). The nucleotide mutations in each SL5 mutant are shown in Fig. 1B. To generate SL5B and SL5C mutants, synonymous mutations that retained the RNA structure were introduced within the loop regions. These constructs were designated as pBAC-MERS-SL5B-Loop and pBAC-MERS-SL5C-Loop, respectively. To generate SL5B-R, SL5C-R, and SL5D-R mutants, synonymous mutations that disrupted RNA structures were introduced into the right side of each stem region, which were designated as pBAC-MERS-SL5B-R, pBAC-MERS-SL5C-R, and pBAC-MERS-SL5D-R, respectively. To retain the RNA secondary structures in each SL, mutations were introduced to the left side of each stem region, yielding SL5B-RL, SL5C-RL, and SL5D-RL, these cDNA clones were designated as pBAC-MERS-SL5B-RL, pBAC-MERS-SL5C-RL, and pBAC-MERS-SL5D-RL, respectively (Fig. 1A,B). Sequence analyses were performed by Eurofins Scientific (Tokyo, Japan) to confirm substitutions.

We established a MERS-CoV replicon system by replacing the genomic sequence between the S and M genes with that of Nluc. A red/ET recombination system counterselection BAC modification kit was used to construct the MERS replicon. To increase Nluc activity, we inserted nts 27,737–27,861 of the MERS-CoV EMC strain, which contain the TRS of the M gene, upstream of Nluc. The cDNA clone of the replicon with the WT sequence was designated as pBAC-MERS-Rep. To construct a polymerase-dead mutant of the MERS replicon, we introduced substitutions (SDD to SAA) within the active site of the viral RNA-dependent RNA polymerase (RdRp; nsp12). In addition, cDNA clones of SL5 mutants were constructed using the method described above.

To establish the reporter MERS coronavirus carrying the ZsGreen gene, the ORF5 gene of the pBAC-MERS-WT was replaced with the ZsGreen gene using the recombination method described above and designated as pBAC-MERS-ZsGreen. Recombination was performed to construct a pBAC-MERS-ZsGreen-SL5D-R cDNA clone carrying the SL5D-R mutation.

Transfection

Huh7 cells were seeded into 6-well plates (Violamo; Misumi, Schaumberg, IL, USA) at 4.0×10^5 cells/well. After incubation at 37 °C overnight, the cells were transfected with 4 µg of cDNA clones using XtremeGene 9 DNA Transfection Reagent (Roche, Basel, Switzerland) according to manufacturer's instructions. After incubating at 37 °C for the indicated time, the culture supernatants and cell pellets were collected and stored at − 80 °C until further use.

Virus rescue and propagation

To propagate reporter viruses, rMERS-ZsGreen and rMERS-ZsGreen-SL5D-R, pBAC-MERS-ZsGreen, or pBAC-MERS-ZsGreen-SL5D-R were transfected into Huh7 cells as described above. After incubating for 3 days, culture supernatants were collected and stored at − 80 °C. Viruses were stored at P0. The rMERS-ZsGreen P0 virus was propagated twice in Vero cells and stored as the P2 virus. The rMERS-ZsGreen-SL5D-R P0 virus was propagated twice in Vero-TMPRSS2 cells and stored as the P2 virus. Viral titers were determined using the titration assay described below.

Titration

The $TCID_{50}$ method using Vero cells was used to determine the infection titer of each virus, as described previously[28].

Realtime RT-PCR

Total RNAs from transfected Huh7 cells were extracted using a PureLink RNA Mini Kit (Thermo Fisher Scientific, Waltham, MA, USA) according to manufacturer's instructions and stored at − 80 °C until use. First-strand cDNA was synthesized using a ReverTra Ace qPCR RT kit (TOYOBO, Osaka, Japan) according to the manufacturer's instructions. For cDNA synthesis, a primer mix (TOYOBO) was used for sg N mRNA, YT750 (5′-GGG CTTGAGGCTTCTCCAATG-3′) was used for positive-strand genomic RNA, and YT749 (5′-ACACTTTTC TTGTTGCCTGTGG-3′) was used for negative-strand genomic RNA. The reverse-transcribed samples were treated with RNase H at 37 °C for 20 min. The level of each cDNA was determined using a Thunderbird Probe qPCR Mix (TOYOBO), and the reaction was performed using a StepOne Real-Time PCR System (Applied Biosystems, Waltham, MA, USA). To quantify the sg N mRNA, we used the primer pair, WK1350 (5′-TCGTTCTCT TGCAGAACTTTG-3′) and WK1351 (5′-TTGGATTACGTCCTCTACCTC-3′), and the FAM-labeled specific probe, WK1352 (5′-CCTCGTGCTGTTTCCTTTGCCGAT-3′). To quantify the positive- or negative-strand genomic RNA, we used the primer pair, YT727 (5′-CCACTACTCCCATTTCGTCAG-3′) and YT728 (5′-CAG TATGTGTAGTGCGCATATAAGCA-3′), and the FAM-labeled specific probe, YT729 (5′-TTGCAAATTGGC TTGCCCCCACT-3′). For quantification of GAPDH mRNA, we used the primer pair, WK1288 (5′-GAAGGT GAAGGTCGGAGT-3′) and WK1289 (5′-GAAGATGGTGATGGGATTTC-3′), and the FAM-labeled specific probe, WK1290 (5′-CAAGCTTCCCGTTCTCAGCC-3′). Cycling conditions were 95 °C for 1 min, followed by 40 cycles of 95 °C for 15 s and 58 °C for 45 s. The RNA levels of GAPDH were used to normalize viral RNA levels.

Immunoblotting

Transfected Huh7 cells were lysed in lysis buffer (100 mM Tris–HCl, pH 8.0, 150 mM NaCl, and 1% TritonX-100). After centrifugation at 16,000×*g*, the supernatants were collected and mixed with 2× sample buffer (0.1 M Tris–HCl pH 6.8, 4% sodium dodecyl sulfate [SDS], 20% glycerol, 0.004% bromophenol blue, and 10% 2-mercaptoethanol). Next, samples were boiled. Proteins were separated by 10% SDS-polyacrylamide gel electrophoresis (SDS-PAGE) and transferred onto a polyvinylidene difluoride (PVDF) membrane (Merck Millipore, Billerica, MA, USA). The membranes were blocked with 3% skim milk in PBS containing 0.05% Tween 20 (Nacalai Tesque). Rabbit anti-MERS-N (Sino Biological, Beijing, China) or mouse anti-β-Actin (Sigma-Aldrich, St. Louis, MO, USA) were used as primary antibodies, and goat anti-mouse IgG-horseradish peroxidase (HRP; Sigma-Aldrich) or goat anti-mouse IgG-HRP (Sigma-Aldrich) were used as secondary antibodies, respectively. ChemiLumi One Ultra (Nacalai Tesque) was used for visualization with the LAS-4000 image analyzer system (Fujifilm, Tokyo, Japan).

Replicon assay

293T cells were seeded into 24-well plates (Violamo) at 1.5×10^5 cells/well and cultured at 37 °C overnight. Next, cDNA clones of the replicon were transfected into seeded 293T cells using XtremeGene 9 DNA Transfection Reagent (Roche) according to the manufacturer's instructions. The firefly luciferase reporter plasmid pGL3-control was co-transfected with each cDNA clone as an internal control. After incubation for 48 h, the transfected cells were lysed using passive buffer (Promega, Madison, WI, USA). Luciferase activity was measured using a PowerScan HT (DS Pharma Biomedical, Osaka, Japan). The Nano-Glo Luciferase Assay System (Promega) was used to measure Nluc activity. A luciferase assay system (Promega) was used to measure firefly luciferase activity. Luciferase activity was normalized to that of firefly luciferase. The experiments were performed in triplicates.

Nsp5 reporter assay

To examine the expression levels of nsp5 in transfected Huh7 cells, we used the biosensor expression plasmid, pGlo-30F-VRLQS[32], which was a kind gift from Dr. Susan Baker (Loyola University, Chicago, IL, USA). pGlo-30F-VRLQS, encoding *Photuris pennsylvanica* luciferase with the inserted amino acid sequence VRLQS, was recognized and cleaved by the MERS nsp5 protease 3CLpro.

Huh7 cells were seeded into 24 well-plates (Violamo) at 1.0×10^5 cells/well and cultured overnight. The seeded cells were transfected with pGlo-30F-VRLQS and cDNA clones using the XtremeGene 9 DNA Transfection Reagent (Roche) according to the manufacturer's instructions. As a control, pBAC-MERS-nsp5-rpsL, in which nsp5 was replaced with an rpsL cassette (Red/ET Recombination System Counter-Selection BAC Modification Kit; Gene Bridges), was used. Transfected cells were cultured for 24 and 48 h and then lysed with passive buffer (Promega). Luciferase activity was measured as previously described.

Correlative light and electron microscopy (CLEM) analysis

Vero cells were seeded into 35-mm glass bottom dishes (P35G-1.5-14-CGRD: MatTek) at 5.0×10^4 cells/well and cultured overnight. Cells were inoculated with rMERS-ZsGreen or rMERS-ZsGreen-SL5D-R at an MOI of 0.1. After adsorption at 37 °C for 1 h, the infected cells were washed with DMEM without FBS and DMEM containing 2% FBS was added. After incubation for 24 h at 37 °C, the laser scanning confocal microscope FluoView FV1000 (Olympus, Tokyo, Japan) was used to observe ZsGreen fluorescence to identify infected cells. Cells were fixed in 4% formaldehyde in 0.1 M phosphate buffer for 30 min at room temperature. Fixed cells were washed three times with washing buffer (4% sucrose in 0.2 M phosphate buffer). After washing, 2.5% glutaraldehyde in 0.1 M phosphate buffer was applied for TEM analysis. Cells were post-fixed for 1 h with 1% osmium tetroxide and 0.5% potassium ferrocyanide in 0.1 M cacodylate buffer (pH 7.4), dehydrated in a graded series of ethanol, and embedded in Epon812 (TAAB, Reading, UK). Ultrathin (80 nm) sections were stained with saturated uranyl acetate and lead citrate solutions. Electron micrographs were acquired using a JEM-1011 transmission electron microscope (JEOL, Tokyo, Japan).

Viral titers in supernatants and cells

Vero cells were seeded into 12-well plates (Violamo) at 2.0×10^5 cells/well and cultured overnight at 37 °C. Cells were inoculated with rMERS-ZsGreen or rMERS-ZsGreen-SL5D-R at a MOI of 0.01. After adsorption at 37 °C for 1 h, the inoculum was removed and 1 mL/well of DMEM containing 2% FBS was added. The infected cells were cultured at 37 °C for 24, 48, and 72 h. Culture supernatants were collected and stored at − 80 °C until use. DMEM containing 2% FBS (1 mL) was added to the cell supernatants, which were then stored at − 80 °C. Freeze–thaw cycles were performed three times, and the samples were centrifuged at 2500×*g* for 10 min. Supernatants were collected as cell samples. The infectious viral titers in the supernatants and cell samples were measured using the $TCID_{50}$ method described above.

Plasmid construction

To construct a luciferase reporter plasmid carrying the MERS-CoV SL5 nucleotide sequence upstream of the firefly luciferase gene, pcDNA3.1-SL5-fluc, we first constructed the plasmid pcDNA3.1-MERS460nt-fluc carrying the first 460 nts of MERS-CoV. Next, the pBAC-MERS was used as a template to amplifying the 460-nt sequence. The PCR product was cloned into pcDNA3.1-fluc[27], and the resulting vector was designated as pcDNA3.1-MERS-460nt-fluc. To construct pcD-SL5-fluc, we deleted nucleotides 1–264 and 349–460 of the MERS-CoV from the pcDNA3.1-MERS-460nt-fluc using the PrimeSTAR mutagenesis kit (Takara Bio, Tokyo, Japan), according to the manufacturer's instructions. To construct the SL5B and SL5C mutants pcDNA3.1-SL5B-R-fluc,

pcDNA3.1-SL5B-RL-fluc, pcDNA3.1-SL5C-R-fluc, and pcDNA3.1-SL5C-RL-fluc, we used the PrimeSTAR mutagenesis kit (Takara) and pcDNA3.1-SL5-fluc as the template.

Luciferase assay

293T cells were seeded into 24-well plates (Violamo) at 1.5×10^5 cells/well and cultured overnight at 37 °C. Cultured cells were transfected with pcDNA3.1, using TransIT LT1 (Mirus, Madison, WI, USA) according to the manufacturer's instructions. Renilla luciferase reporter plasmid pRL-SV40 was used as an internal control. At 24 h post-transfection, the transfected cells were lysed with passive buffer (Promega) and luciferase activity was measured as described above. The firefly luciferase activity was normalized to the Renilla luciferase activity.

Viral passage in Vero cells

Vero cells were seeded into 10 cm dishes (Violamo) at 2.0×10^6 cells/well and cultured overnight at 37 °C. Seeded Vero cells were inoculated with rMERS-SL5D-R P0 virus and allowed to adsorb for 1 h. After adsorption, the inoculated cells were washed twice with DMEM and 10 mL of DMEM containing 2% FBS was added. The cells were cultured for 3 days and cytopathic effects (CPEs) were observed. The supernatant was collected and stored at − 80 °C as P1 virus. The rMERS-SL5D-R P1 virus was further amplified nine times in Vero cells (P10 virus) and viruses from each amplification were stored at − 80 °C. Viral titers were determined using the $TCID_{50}$ assay described above.

Growth kinetics of passaged rMERS-SL5D-R viruses in Vero cells

Vero cells were seeded into 6-well plates (Violamo) at 4.0×10^5 cells/well and cultured overnight at 37 °C. Cultured cells were inoculated with rMERS-WT or rMERS-SL5D-R (P1, P2, P5, or P10) viruses at an MOI of 0.01. After adsorption, the cells were washed twice with DMEM and 2 mL of DMEM containing 2% FBS was added to each well. The infected cells were cultured for 24, 48, and 72 h, and the supernatants were collected and stored at − 80 °C until use. Viral titers of the culture supernatants were determined using the $TCID_{50}$ assay described above.

Plaque assay

Vero cells were seeded into 6-well plates (Violamo) at 6.0×10^5 cells/well and cultured overnight at 37 °C. Cultured Vero cells were inoculated at a $TCID_{50}$ of 25 and passaged rMERS-SL5D-R (P2, P5, or P10) viruses. After adsorption at 37 °C for 1 h, the cells were washed twice with DMEM and then overlaid with 0.8% agarose (Seaplaque® GTG Agarose; Lonza, Switzerland) in DMEM containing 2% FBS. Infected cells were cultured at 37 °C for 3 days and then fixed with phosphate-buffered formalin. Fixed cells were stained with crystal violet.

LRIscan

To construct the RNA alignment data for LRIscan[33], we used Molecular Evolutionary Genetics Analysis version 6.0 (MEGA6[49]). To construct the MERS-CoV alignment data, we used the full-length sequences of four MERS-CoV strains: MERS-CoV_EMC (Accession No.: NC_019843), MERS-CoV Hu/Oman_50_2015 (Accession No.: KY673148.1), MERS-CoV Al-Hasa_1_2013 (Accession No.: KY673148.1), and MERS-CoV Korea/Seoul/SNU1-035/2015 (Accession No.: KY673148.1). The cluster file containing MERS-CoV alignment data was analyzed using LRIscan[33] and plotted with Circos[50].

Statistical analyses

A two-way analysis of variance (ANOVA) test was conducted to determine statistical significance using GraphPad Prism ver. 10 (GraphPad Software, San Diego, CA, USA). A p value of < 0.05 was considered statistically significant.

Data availability

The datasets used and/or analysed during the current study available from the corresponding author on reasonable request.

Received: 8 February 2024; Accepted: 19 August 2024
Published online: 23 August 2024

References

1. Weiss, S. R. & Navas-Martin, S. Coronavirus pathogenesis and the emerging pathogen severe acute respiratory syndrome coronavirus. *Microbiol. Mol. Biol. Rev.* **69**, 635–664. https://doi.org/10.1128/MMBR.69.4.635-664.2005 (2005).
2. Bradburne, A. F., Bynoe, M. L. & Tyrrell, D. A. Effects of a "new" human respiratory virus in volunteers. *Br. Med. J.* **3**, 767–769. https://doi.org/10.1136/bmj.3.5568.767 (1967).
3. van der Hoek, L., Pyrc, K. & Berkhout, B. Human coronavirus NL63, a new respiratory virus. *FEMS Microbiol. Rev.* **30**, 760–773. https://doi.org/10.1111/j.1574-6976.2006.00032.x (2006).
4. van der Hoek, L. *et al.* Identification of a new human coronavirus. *Nat. Med.* **10**, 368–373. https://doi.org/10.1038/nm1024 (2004).
5. Woo, P. C. *et al.* Characterization and complete genome sequence of a novel coronavirus, coronavirus HKU1, from patients with pneumonia. *J. Virol.* **79**, 884–895. https://doi.org/10.1128/JVI.79.2.884-895.2005 (2005).
6. Drosten, C. *et al.* Identification of a novel coronavirus in patients with severe acute respiratory syndrome. *N. Engl. J. Med.* **348**, 1967–1976. https://doi.org/10.1056/NEJMoa030747 (2003).
7. Ksiazek, T. G. *et al.* A novel coronavirus associated with severe acute respiratory syndrome. *N. Engl. J. Med.* **348**, 1953–1966. https://doi.org/10.1056/NEJMoa030781 (2003).
8. Zaki, A. M., van Boheemen, S., Bestebroer, T. M., Osterhaus, A. D. & Fouchier, R. A. Isolation of a novel coronavirus from a man with pneumonia in Saudi Arabia. *N. Engl. J. Med.* **367**, 1814–1820. https://doi.org/10.1056/NEJMoa1211721 (2012).

9. Chen, N. *et al.* Epidemiological and clinical characteristics of 99 cases of 2019 novel coronavirus pneumonia in Wuhan, China: A descriptive study. *Lancet* **395**, 507–513. https://doi.org/10.1016/S0140-6736(20)30211-7 (2020).
10. Huang, C. *et al.* Clinical features of patients infected with 2019 novel coronavirus in Wuhan, China. *Lancet* **395**, 497–506. https://doi.org/10.1016/S0140-6736(20)30183-5 (2020).
11. Wang, D. *et al.* Clinical characteristics of 138 hospitalized patients with 2019 novel coronavirus-infected pneumonia in Wuhan, China. *JAMA* **323**, 1061–1069. https://doi.org/10.1001/jama.2020.1585 (2020).
12. Ferhadian, D. *et al.* Structural and functional motifs in influenza virus RNAs. *Front. Microbiol.* **9**, 559. https://doi.org/10.3389/fmicb.2018.00559 (2018).
13. Ito, T., Tahara, S. M. & Lai, M. M. The 3′-untranslated region of hepatitis C virus RNA enhances translation from an internal ribosomal entry site. *J. Virol.* **72**, 8789–8796. https://doi.org/10.1128/JVI.72.11.8789-8796.1998 (1998).
14. Tsukiyama-Kohara, K., Iizuka, N., Kohara, M. & Nomoto, A. Internal ribosome entry site within hepatitis C virus RNA. *J. Virol.* **66**, 1476–1483. https://doi.org/10.1128/JVI.66.3.1476-1483.1992 (1992).
15. Villordo, S. M., Carballeda, J. M., Filomatori, C. V. & Gamarnik, A. V. RNA structure duplications and flavivirus host adaptation. *Trends Microbiol.* **24**, 270–283. https://doi.org/10.1016/j.tim.2016.01.002 (2016).
16. Jang, S. K. *et al.* A segment of the 5′ nontranslated region of encephalomyocarditis virus RNA directs internal entry of ribosomes during in vitro translation. *J. Virol.* **62**, 2636–2643. https://doi.org/10.1128/JVI.62.8.2636-2643.1988 (1988).
17. Pelletier, J. & Sonenberg, N. Internal initiation of translation of eukaryotic mRNA directed by a sequence derived from poliovirus RNA. *Nature* **334**, 320–325. https://doi.org/10.1038/334320a0 (1988).
18. Sola, I., Almazan, F., Zuniga, S. & Enjuanes, L. Continuous and discontinuous RNA synthesis in coronaviruses. *Annu. Rev. Virol.* **2**, 265–288. https://doi.org/10.1146/annurev-virology-100114-055218 (2015).
19. Yang, D. & Leibowitz, J. L. The structure and functions of coronavirus genomic 3′ and 5′ ends. *Virus Res.* **206**, 120–133. https://doi.org/10.1016/j.virusres.2015.02.025 (2015).
20. Fosmire, J. A., Hwang, K. & Makino, S. Identification and characterization of a coronavirus packaging signal. *J. Virol.* **66**, 3522–3530. https://doi.org/10.1128/JVI.66.6.3522-3530.1992 (1992).
21. Chen, S. C. & Olsthoorn, R. C. Group-specific structural features of the 5′-proximal sequences of coronavirus genomic RNAs. *Virology* **401**, 29–41. https://doi.org/10.1016/j.virol.2010.02.007 (2010).
22. Kim, Y. N. & Makino, S. Characterization of a murine coronavirus defective interfering RNA internal cis-acting replication signal. *J. Virol.* **69**, 4963–4971. https://doi.org/10.1128/JVI.69.8.4963-4971.1995 (1995).
23. Liu, P. *et al.* A U-turn motif-containing stem-loop in the coronavirus 5′ untranslated region plays a functional role in replication. *RNA* **13**, 763–780. https://doi.org/10.1261/rna.261807 (2007).
24. Raman, S., Bouma, P., Williams, G. D. & Brian, D. A. Stem-loop III in the 5′ untranslated region is a cis-acting element in bovine coronavirus defective interfering RNA replication. *J. Virol.* **77**, 6720–6730. https://doi.org/10.1128/jvi.77.12.6720-6730.2003 (2003).
25. Raman, S. & Brian, D. A. Stem-loop IV in the 5′ untranslated region is a cis-acting element in bovine coronavirus defective interfering RNA replication. *J. Virol.* **79**, 12434–12446. https://doi.org/10.1128/JVI.79.19.12434-12446.2005 (2005).
26. Yang, D., Liu, P., Wudeck, E. V., Giedroc, D. P. & Leibowitz, J. L. SHAPE analysis of the RNA secondary structure of the Mouse Hepatitis Virus 5′ untranslated region and N-terminal nsp1 coding sequences. *Virology* **475**, 15–27. https://doi.org/10.1016/j.virol.2014.11.001 (2015).
27. Tanaka, T., Kamitani, W., DeDiego, M. L., Enjuanes, L. & Matsuura, Y. Severe acute respiratory syndrome coronavirus nsp1 facilitates efficient propagation in cells through a specific translational shutoff of host mRNA. *J. Virol.* **86**, 11128–11137. https://doi.org/10.1128/JVI.01700-12 (2012).
28. Terada, Y., Kawachi, K., Matsuura, Y. & Kamitani, W. MERS coronavirus nsp1 participates in an efficient propagation through a specific interaction with viral RNA. *Virology* **511**, 95–105. https://doi.org/10.1016/j.virol.2017.08.026 (2017).
29. Kim, Y. N., Jeong, Y. S. & Makino, S. Analysis of cis-acting sequences essential for coronavirus defective interfering RNA replication. *Virology* **197**, 53–63. https://doi.org/10.1006/viro.1993.1566 (1993).
30. Zuker, M. Mfold web server for nucleic acid folding and hybridization prediction. *Nucleic Acids Res.* **31**, 3406–3415. https://doi.org/10.1093/nar/gkg595 (2003).
31. Snijder, E. J., Decroly, E. & Ziebuhr, J. The nonstructural proteins directing coronavirus RNA synthesis and processing. *Adv. Virus Res.* **96**, 59–126. https://doi.org/10.1016/bs.aivir.2016.08.008 (2016).
32. Kilianski, A., Mielech, A. M., Deng, X. & Baker, S. C. Assessing activity and inhibition of Middle East respiratory syndrome coronavirus papain-like and 3C-like proteases using luciferase-based biosensors. *J. Virol.* **87**, 11955–11962. https://doi.org/10.1128/JVI.02105-13 (2013).
33. Fricke, M. & Marz, M. Prediction of conserved long-range RNA–RNA interactions in full viral genomes. *Bioinformatics* **32**, 2928–2935. https://doi.org/10.1093/bioinformatics/btw323 (2016).
34. Shirogane, Y. *et al.* Efficient multiplication of human metapneumovirus in Vero cells expressing the transmembrane serine protease TMPRSS2. *J. Virol.* **82**, 8942–8946. https://doi.org/10.1128/JVI.00676-08 (2008).
35. Goebel, S. J., Hsue, B., Dombrowski, T. F. & Masters, P. S. Characterization of the RNA components of a putative molecular switch in the 3′ untranslated region of the murine coronavirus genome. *J. Virol.* **78**, 669–682. https://doi.org/10.1128/jvi.78.2.669-682.2004 (2004).
36. Goebel, S. J., Taylor, J. & Masters, P. S. The 3′ cis-acting genomic replication element of the severe acute respiratory syndrome coronavirus can function in the murine coronavirus genome. *J. Virol.* **78**, 7846–7851. https://doi.org/10.1128/JVI.78.14.7846-7851.2004 (2004).
37. Dickson, A. M. & Wilusz, J. Strategies for viral RNA stability: Live long and prosper. *Trends Genet.* **27**, 286–293. https://doi.org/10.1016/j.tig.2011.04.003 (2011).
38. Ford, L. P. & Wilusz, J. 3′-Terminal RNA structures and poly(U) tracts inhibit initiation by a 3′–>5′ exonuclease in vitro. *Nucleic Acids Res.* **27**, 1159–1167. https://doi.org/10.1093/nar/27.4.1159 (1999).
39. Sawicki, S. G. & Sawicki, D. L. A new model for coronavirus transcription. *Adv. Exp. Med. Biol.* **440**, 215–219. https://doi.org/10.1007/978-1-4615-5331-1_26 (1998).
40. Sola, I., Mateos-Gomez, P. A., Almazan, F., Zuniga, S. & Enjuanes, L. RNA–RNA and RNA–protein interactions in coronavirus replication and transcription. *RNA Biol.* **8**, 237–248. https://doi.org/10.4161/rna.8.2.14991 (2011).
41. Sola, I., Moreno, J. L., Zuniga, S., Alonso, S. & Enjuanes, L. Role of nucleotides immediately flanking the transcription-regulating sequence core in coronavirus subgenomic mRNA synthesis. *J. Virol.* **79**, 2506–2516. https://doi.org/10.1128/JVI.79.4.2506-2516.2005 (2005).
42. Zuniga, S., Sola, I., Alonso, S. & Enjuanes, L. Sequence motifs involved in the regulation of discontinuous coronavirus subgenomic RNA synthesis. *J. Virol.* **78**, 980–994. https://doi.org/10.1128/jvi.78.2.980-994.2004 (2004).
43. Spagnolo, J. F. & Hogue, B. G. Host protein interactions with the 3′ end of bovine coronavirus RNA and the requirement of the poly(A) tail for coronavirus defective genome replication. *J. Virol.* **74**, 5053–5065. https://doi.org/10.1128/jvi.74.11.5053-5065.2000 (2000).
44. Nelson, G. W., Stohlman, S. A. & Tahara, S. M. High affinity interaction between nucleocapsid protein and leader/intergenic sequence of mouse hepatitis virus RNA. *J. Gen. Virol.* **81**, 181–188. https://doi.org/10.1099/0022-1317-81-1-181 (2000).
45. Zuniga, S. *et al.* Coronavirus nucleocapsid protein facilitates template switching and is required for efficient transcription. *J. Virol.* **84**, 2169–2175. https://doi.org/10.1128/JVI.02011-09 (2010).

46. Zuniga, S. *et al.* Coronavirus nucleocapsid protein is an RNA chaperone. *Virology* **357**, 215–227. https://doi.org/10.1016/j.virol.2006.07.046 (2007).
47. Kuo, L., Koetzner, C. A., Hurst, K. R. & Masters, P. S. Recognition of the murine coronavirus genomic RNA packaging signal depends on the second RNA-binding domain of the nucleocapsid protein. *J. Virol.* **88**, 4451–4465. https://doi.org/10.1128/JVI.03866-13 (2014).
48. Guan, B. J., Wu, H. Y. & Brian, D. A. An optimal cis-replication stem-loop IV in the 5′ untranslated region of the mouse coronavirus genome extends 16 nucleotides into open reading frame 1. *J. Virol.* **85**, 5593–5605. https://doi.org/10.1128/JVI.00263-11 (2011).
49. Tamura, K., Stecher, G., Peterson, D., Filipski, A. & Kumar, S. MEGA6: Molecular Evolutionary Genetics Analysis version 6.0. *Mol. Biol. Evol.* **30**, 2725–2729. https://doi.org/10.1093/molbev/mst197 (2013).
50. Krzywinski, M. *et al.* Circos: An information aesthetic for comparative genomics. *Genome Res.* **19**, 1639–1645. https://doi.org/10.1101/gr.092759.109 (2009).

Acknowledgements
We thank Dr. Luis Enjuanes (CNB-CSIC, Madrid, Spain) for providing the BAC DNA reagent, and Dr. Bart L. Haagmens (Erasmus Medical Center, Rotterdam, Netherlands) for providing the MERS-CoV/EMC2012 strain through Dr. Makoto Takeda (National Institute of Infectious Diseases). We also thank Dr. Susan C. Baker (Loyola University, Chicago, IL, USA) for providing us with the MERS protease reporter system. We thank Ms. Kaede Yukawa and Marie Shitara for secretarial assistance and Ms. Kanako Yoshizawa, Nozomi Shimada, Yuki Shida, Yukari Shiba, and Naho Takashima for their technical assistance. We also thank Dr. Naohisa Goto for advice on the LRIscan analyses and Dr. Hiroko Omori for the electron microscopy analyses.

Author contributions
Y.T. and W.K. conceived and designed the experiments. Y. T., and S. A. performed the experiments. Y.T., Y.M., and W.K. analyzed the data and wrote the manuscript.

Funding
This study was supported by a Grant for Joint Research Project of the Research Institute for Microbial Diseases, Osaka University. This work was supported in part by grants-in-aid from the Japanese Society for the Promotion of Science (JSPS), KAKENHI grant (JP16K08811and JP15J07066), from the Ministry of Health, Labor and Welfare of Japan, and the Japan Agency for Medical Research and Development (AMED, JP18fk0108058, JP18fm028101j0002, JP21fk0108560h, and JP20fk0108267h). This work was supported in part by the Japan Science and Technology Agency (Moonshot Research & Development) (Grant Number JPMJMS2025). YT was supported by a JSPS Research Fellowship for Young Scientists.

Competing interests
The authors declare no competing interests.

Additional information
Supplementary Information The online version contains supplementary material available at https://doi.org/10.1038/s41598-024-70601-5.

Correspondence and requests for materials should be addressed to W.K.

Reprints and permissions information is available at www.nature.com/reprints.

Publisher's note Springer Nature remains neutral with regard to jurisdictional claims in published maps and institutional affiliations.